SCIENCE CHINA PRESS

SCIENCE CHINA Life Sciences
life.scichina.com link.springer.com
https://doi.org/10.1007/s11427-024-2703-6

RESEARCH PAPER

Targeting STING oligomerization with licochalcone D ameliorates STING-driven inflammatory diseases

Yinghui Zhang[1,2†], Yadan Liu[1,3†], Bing Jiang[3†], Lifan Chen[1,2], Jie Hu[3], Buying Niu[1,2], Jie Chang[1], Zisheng Fan[1,5], Jingyi Zhou[1,6], Yajie Wang[2,4], Dan Teng[1,2], Ning Ma[2,4], Xiaofeng Wang[2,4], Ruirui Yang[2,4*], Mingyue Zheng[1,2,3,4,5,6,7*] & Sulin Zhang[1,2*]

[1]Drug Discovery and Design Center, State Key Laboratory of Drug Research, Shanghai Institute of Materia Medica, Chinese Academy of Sciences, Shanghai 201203, China;
[2]University of Chinese Academy of Sciences, Beijing 100049, China;
[3]School of Chinese Materia Medica, Nanjing University of Chinese Medicine, Nanjing 210023, China;
[4]School of Pharmaceutical Science and Technology, Hangzhou Institute for Advanced Study, University of Chinese Academy of Sciences, Hangzhou 310024, China;
[5]Shanghai Institute for Advanced Immunochemical Studies, and School of Life Science and Technology, Shanghai Tech University, Shanghai 200031, China;
[6]School of Physical Science and Technology, ShanghaiTech University, Shanghai 200031, China;
[7]State Key Laboratory of Pharmaceutical Biotechnology, Nanjing University, Nanjing 210023, China

†Contributed equally to this work
*Corresponding authors (Sulin Zhang, email: slzhang@simm.ac.cn; Mingyue Zheng, email: myzheng@simm.ac.cn; Ruirui Yang, email: yangruirui@simm.ac.cn)

Received 8 April 2024; Accepted 9 August 2024; Published online 22 August 2024

The development of STING inhibitors for the treatment of STING-related inflammatory diseases continues to encounter significant challenges. The activation of STING is a multi-step process that includes binding with cGAMP, self-oligomerization, and translocation from the endoplasmic reticulum to the Golgi apparatus, ultimately inducing the expression of IRF3 and NF-κB-mediated interferons and inflammatory cytokines. It has been demonstrated that disruption of any of these steps can effectively inhibit STING activation. Traditional structure-based drug screening methodologies generally focus on specific binding sites. In this study, a TransformerCPI model based on protein primary sequences and independent of binding sites is employed to identify compounds capable of binding to the STING protein. The natural product Licochalcone D (LicoD) is identified as a potent and selective STING inhibitor. LicoD does not bind to the classical ligand-binding pocket; instead, it covalently modifies the Cys148 residue of STING. This modification inhibits STING oligomerization, consequently suppressing the recruitment of TBK1 and the nuclear translocation of IRF3 and NF-κB. LicoD treatment ameliorates the inflammatory phenotype in *Trex1*$^{-/-}$ mice and inhibits the progression of DSS-induced colitis and AOM/DSS-induced colitis-associated colon cancer (CAC). In summary, this study reveals the potential of LicoD in treating STING-driven inflammatory diseases. It also demonstrates the utility of the TransformerCPI model in discovering allosteric compounds beyond the conventional binding pockets.

cGAS-STING signaling | STING inhibitor | TransformerCPI model | Licochalcone D | inflammatory diseases

INTRODUCTION

The cyclic GMP–AMP synthase (cGAS)–stimulator of interferon genes (STING) pathway senses abnormal cytoplasmic DNA and then initiates host immune responses against invading pathogens and cancer. The double-stranded DNA (dsDNA) originating from microbes and host cells triggers the activation of cGAS, leading to the production of the second messenger 2′3′ cyclic GMP-AMP (cGAMP) from adenosine triphosphate (ATP) and guanosine triphosphate (GTP) (Ablasser et al., 2013; Paludan and Bowie, 2013; Wang et al., 2020; Wu et al., 2013). cGAMP in turn binds to and activates STING on the endoplasmic reticulum (ER) (Barber, 2015; Hopfner and Hornung, 2020; Shang et al., 2019). Then, activated STING forms oligomerization and translocates to the Golgi apparatus to activate TANK-binding kinase 1 (TBK1) and IκB kinase (IKK), which phosphorylate and activate interferon regulatory factor 3 (IRF3) and nuclear factor kappa-B (NF-κB) (Abe and Barber, 2014; Tanaka and Chen, 2012; Yum et al., 2021; Zhang et al., 2019; Zhao et al., 2019). The translocation of activated IRF3 and NF-κB into the cell nucleus induces the production of type I interferons (IFNs) and pro-inflammatory cytokines, leading to innate immune responses (Liu et al., 2015). Thus, the cGAS-STING signaling is essential for host defense against microbial infection and anti-tumor immunity (Zheng et al., 2020).

However, abnormal or excessive activation of cGAS-STING signaling can lead to a variety of inflammatory and autoimmune diseases (Motwani et al., 2019). Loss-of-function mutations in *TREX1* (encoding DNase III) or *DNASE2* (encoding DNase II) can cause the accumulation of cytoplastic DNA, which results in sustained activation of cGAS-STING pathway (Motwani et al., 2019). People with these mutations may develop into Aicardi-Goutières syndrome (AGS) or systemic lupus erythematosus (SLE) (Crow and Manel, 2015; Gray et al., 2015; Rodero et al., 2017). In *Trex1*$^{-/-}$ mice, deletion or pharmacological inhibition of STING greatly attenuates the inflammatory phenotypes (Ahn et al., 2014; Haag et al., 2018). Likewise, gain-of-function mutations in STING, which induce STING self-activation in the absence of cGAMP, can also result in a severe autoimmune disease called STING-associated vasculopathy with onset in infancy (SAVI) (Liu et al., 2014). It has also been reported that abnormal activation of STING signaling was involved in the

CrossMark click for updates

pathogenesis of inflammatory bowel disease (IBD) (Ahn et al., 2017; Zhao et al., 2021). Commensal bacterial and exosomal dsDNA activate cGAS-STING pathway and trigger intestinal inflammation, and STING deficiency significantly ameliorates the inflammatory phenotypes (Ahn et al., 2017; Zhao et al., 2021). In addition, senescent cells with aberrant cytosolic chromatin fragments can activate cGAS-STING pathway to promote the production of senescence-associated secretory phenotype (SASP), thereby driving paracrine senescence (Glück et al., 2017; Gulen et al., 2023; Yang et al., 2017a). This senescent phenotype is impaired with the deficiency of cGAS or STING (Glück et al., 2017; Gulen et al., 2023; Yang et al., 2017a). These studies collectively emphasize the significant contributions of STING in autoimmune and inflammatory diseases, indicating that inhibition of STING is a promising therapeutic approach for inflammatory disorders.

Currently, the design and development of STING inhibitors primarily involve targeting the ligand-binding pocket to compete with cGAMP binding, exemplified by compounds like Astin C and SN-011 (Hong et al., 2021; Li et al., 2018). Additionally, inhibiting the palmitoylation of STING at Cys88/Cys91 to disrupt its localization on the Golgi apparatus can also impede STING activation, with representative compounds including C176 and H151 (Haag et al., 2018). Recent study has reported that BB-Cl-amidine, a cysteine-reactive molecule, covalently modifies multiple cysteine residues of STING, including Cys148, Cys206, Cys257, and Cys309 (Humphries et al., 2023). Given the significance of Cys148 in STING oligomerization, BB-Cl-amidine effectively inhibits the activation of the STING signaling pathway (Ergun et al., 2019; Humphries et al., 2023). These inhibitors can suppress cellular STING signaling activation and mitigate the inflammatory phenotype in *Trex1*-null mice (Haag et al., 2018; Hong et al., 2021; Humphries et al., 2023; Li et al., 2018). However, due to issues such as poor pharmacokinetics and insufficient *in vivo* activity, none of these inhibitors have progressed to clinical studies.

In this study, sequence-based artificial intelligence (AI) virtual screening (Chen et al., 2020), combined with biochemical methods, identified the natural product Licochalcone D (LicoD) as a potent and selective STING inhibitor. LicoD disrupted STING oligomerization through covalent modification of Cys148. Therefore, LicoD could inhibit the activation of STING signaling triggered by agonists or SAVI-related variants. Importantly, LicoD attenuated the inflammatory response in *Trex1*$^{-/-}$ mice and ameliorated DSS-induced colitis and AOM/DSS-induced colitis-associated colon cancer (CAC). These findings collectively suggested the potential therapeutic application of LicoD in STING-related inflammatory and autoimmune diseases.

RESULTS

Sequence-based AI virtual screening for STING inhibitors

The activation of STING signaling pathway involves multiple steps: initially, the binding of STING dimer to agonists, followed by oligomerization; subsequently, translocation to the Golgi membrane occurs, accompanied by the recruitment of TBK1 and IRF3 (Hopfner and Hornung, 2020). Disruption of any of these steps can effectively inhibit STING activation (Haag et al., 2018; Hong et al., 2021; Humphries et al., 2023; Li et al., 2018). This provides several strategic possibilities and multiple potential binding sites for the development of STING inhibitors. Traditional structure-based drug screening methodologies generally focus on specific binding sites. To fully utilize STING's multiple binding sites, we employed the TransformerCPI model for the virtual screening. This model is a protein primary sequence-based, binding site-independent, end-to-end deep learning model (Chen et al., 2020). The optimized TransformerCPI model was utilized to evaluate the potential interaction between STING and 200,000 compounds from SPECS and our in-house library. To ensure molecular diversity, the top 1,000 compounds, ranked according to their AI scores, were clustered using extended-connectivity fingerprints (ECFPs). This process resulted in 100 distinct clusters. Within each cluster, the compound with the highest AI score was selected as the representative molecule for subsequent study (Figure 1A; Table S1 in Supporting Information).

The protein thermal shift (PTS) assay was firstly utilized to detect the binding activity of these 100 candidates to the carboxy-terminal domain of the human STING H232 allele (hSTING^{H232}). Among these candidates, the natural product Licochalcone D (LicoD) increased the thermal stability of hSTING^{H232} in a dose-dependent manner (Figure 1B and C). Additionally, LicoD also increased the thermal stability of human STING R232 allele (hSTING^{R232}), human STING self-activating mutants (hSTING^{S154} and hSTING^{M155}), and murine STING (mSTING) in a dose-dependent manner (Figure 1D; Figure S1A–D in Supporting Information). The surface plasmon resonance (SPR) assay was further employed to determine the binding affinity of LicoD to the STING proteins. The results indicated that LicoD directly binds to both hSTING^{H232} and hSTING^{R232} with K_D values 1.18 and 3.67 μmol L^{-1}, respectively (Figure 1E; Figure S1E in Supporting Information). To further confirm the binding of LicoD to STING protein, the isothermal titration calorimetry (ITC) experiment, a robust method for determining protein-ligand interactions and thermodynamic parameters, was conducted. The K_D value between LicoD and hSTING^{H232} was 2.26 μmol L^{-1}, with the enthalpy change (ΔH) and entropy change (-TΔS) being −34.9 and 2.64 kJ mol^{-1}, respectively, and the stoichiometry of binding (N) being 1.01 (Figure 1F). Collectively, these data suggest that LicoD, a nature product derived from licorice, can directly bind to STING protein.

LicoD selectively inhibits the activation of cGAS-STING signaling by directly inhibiting STING

To determine the effect of LicoD on intracellular cGAS-STING signaling, we first examined its impact on the transcriptional levels of *IFNB1*, *CXCL10* and *IL6* mRNA in dsDNA-stimulated THP-1 derived macrophages and RAW264.7 cells. As shown in Figure 2A and B, LicoD exhibited a dose-dependent inhibitory effect on the expression of these genes in both cell types stimulated with dsDNA. Additionally, LicoD dose-dependently reduced the reporter signals induced by endogenous STING ligand cGAMP in THP1-Blue ISG and RAW-Lucia ISG cells, with IC_{50} values of 2.75 and 0.32 μmol L^{-1}, respectively (Figure 2C). Considering that cGAS acts upstream of STING, and LicoD can inhibit signaling induced by both cGAS and STING activation, it suggests that LicoD inhibits either STING itself or its downstream components, rather than cGAS. To ascertain whether LicoD specifically targets STING or its downstream components, the overexpression of STING, TBK1 and IRF3-5D genes was

https://doi.org/10.1007/s11427-024-2703-6

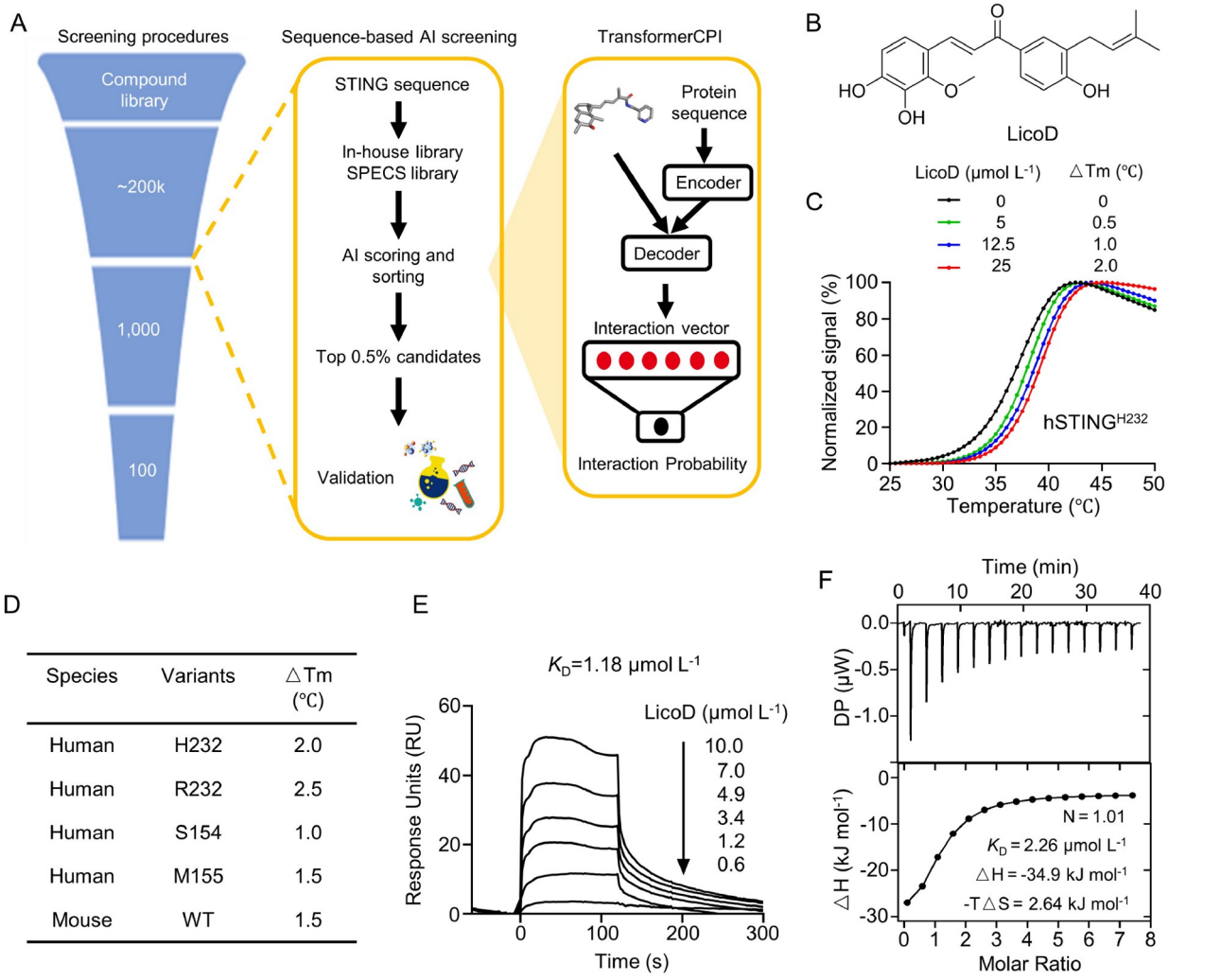

D

Species	Variants	△Tm (℃)
Human	H232	2.0
Human	R232	2.5
Human	S154	1.0
Human	M155	1.5
Mouse	WT	1.5

Figure 1. Sequence-based AI virtual screening for STING inhibitors. A, Sequence-based discovery of small-molecule compounds targeting STING. B, The chemical structure of LicoD. C, Effect of the indicated concentration of LicoD on the thermal stability of hSTING^{H232} (2.5 μmol L^{-1}) in the PTS assay. D, Summary of the impact of LicoD on the thermal stability of different hSTING variants and mSTING protein. E, The kinetics of LicoD binding to hSTING^{H232} was tested by SPR assay. F, The ITC assay was used to test the binding affinity of LicoD to hSTING^{H232}.

employed to induce *IFNB1* transcription in 293T cells in the presence or absence of LicoD. Notably, LicoD dose-dependently reduced STING-mediated *IFNB1* mRNA expression, but not those mediated by TBK1 or IRF3-5D (Figure 2D). Given the hierarchical relationship among these signaling components, these results suggest that LicoD hinders the activation of cGAS-STING signaling by directly inhibiting STING in cells. This was further supported by LicoD's potent reduction in the transcription of pro-inflammatory cytokines and phosphorylation of key components in the STING pathway induced by cGAMP, hydrolysis-resistant cyclic dinucleotide (CDN) analogues (ADU-S100), and non-CDN small molecule agonists (diABZI and SR-717) in THP-1 derived macrophages and RAW264.7 cells (Figure 2E–G; Figure S2A–F in Supporting Information). Global transcriptomic analysis of THP-1 derived macrophages demonstrated that LicoD markedly attenuated cGAMP-induced expression of IFN and pro-inflammatory cytokines (Figure 2H). Importantly, LicoD alone did not induce significant alterations in the transcriptional profile of THP-1-derived macrophages compared to the DMSO-treated group (Figure 2H). Differential gene set enrichment analysis (GSEA) further substantiated the inhibitory capability of LicoD on STING-mediated signaling. The three most prominently down-regulated gene sets in the LicoD plus cGAMP group, in comparison to the cGAMP alone group, were associated with 'interferon gamma response', 'interferon alpha response', and 'inflammatory response' (Figure 2I). It's worth noting that LicoD did not reduce the elevated levels of inflammatory cytokine mRNA induced by poly (I:C) (TLR3 agonist), Lipopolysaccharide (LPS, TLR4 agonist), Pam3CSK4 (TLR1/2 agonist), Zymosan A (TLR2 agonist), or Interleukin-1 beta (IL-1β, CD121a agonist) (Figure 2E and F; Figure S3A–D in Supporting Information). Additionally, LicoD within the specified administration concentration range showed no obvious cytotoxicity in THP-1 derived macrophages and RAW264.7 cells (Figure S4A and B in Supporting Information). Collectively, these results strongly suggest that LicoD selectively inhibited the activation of the intracellular cGAS-STING signaling pathway by directly inhibiting STING.

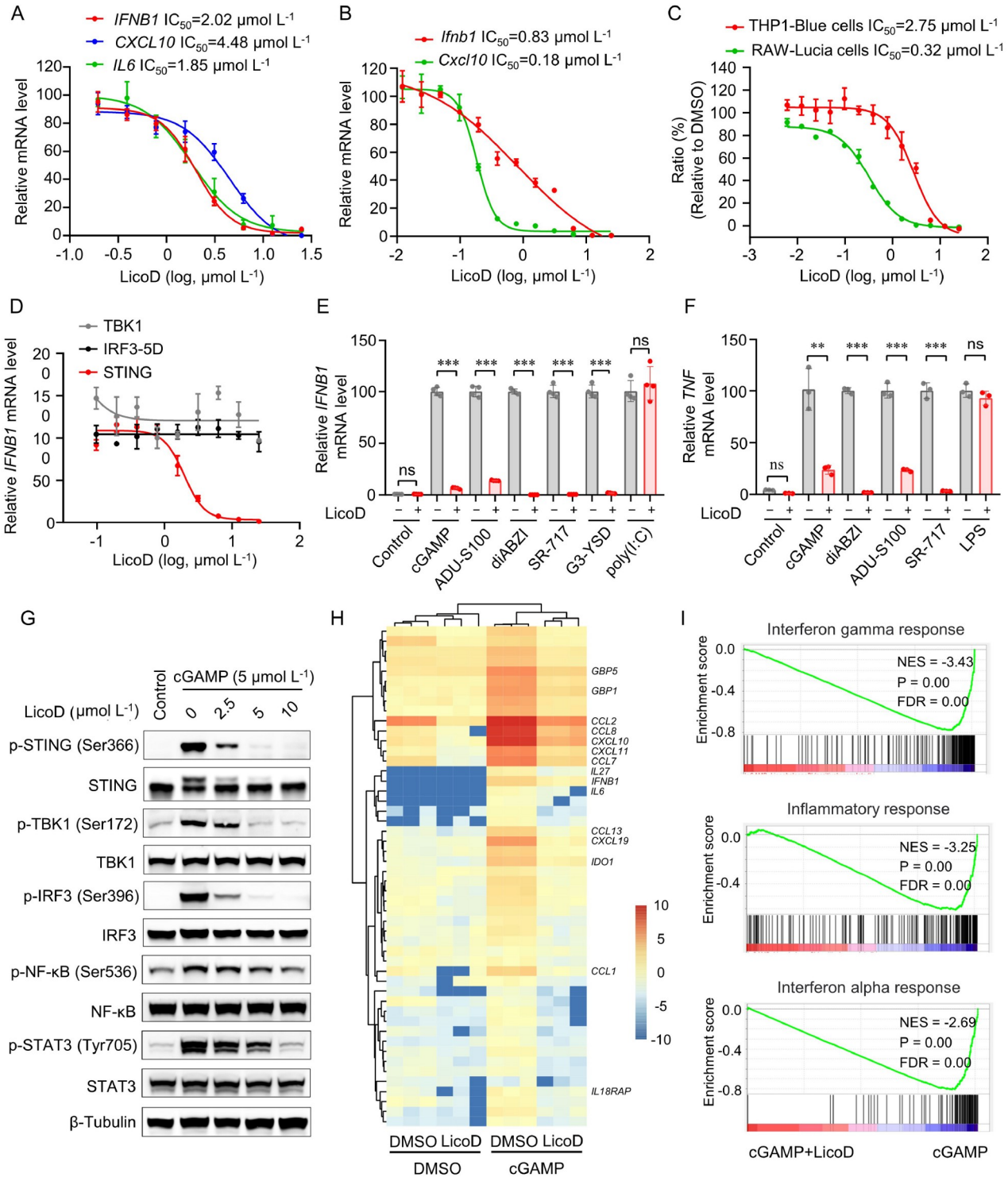

Figure 2. LicoD selectively inhibits the activation of cGAS-STING signaling by directly inhibiting STING. A and B, THP-1 derived macrophages (A) and RAW264.7 cells (B) were pretreated with the indicated concentration of LicoD prior to dsDNA (G3-YSD or ISD) stimulation for 2 h. After 6 h, the *IFNB1*, *CXCL10* and *IL6* mRNA levels were measured by RT-qPCR. C, THP1-Blue ISG cells and RAW-Lucia ISG cells were treated with the indicated concentration of LicoD and cGAMP (2 μmol L^{-1}) for 24 h, subsequently followed by the detection of SEAP and luciferase reporter activity. D, 293T cells were firstly transfected with STING, TBK1 or IRF3-5D plasmids for 24 h and subsequently treated with the indicated concentration of LicoD for 6 h. The *IFNB1* mRNA level was measured by RT-qPCR. E and F, THP-1 derived macrophages were co-treated with 10 μmol L^{-1} LicoD and cGAMP (2 μmol L^{-1}), ADU-S100 (1 μmol L^{-1}), diABZI (100 nmol L^{-1}), SR-717 (5 μmol L^{-1}), G3-YSD, poly (I:C), or LPS. The *IFNB1* (E) and *TNF* (F) mRNA levels were measured by RT-qPCR after 6 h. G, THP-1 derived macrophages were co-treated with the indicated concentration of LicoD and cGAMP for 2 h. Subsequently, cells were analyzed for the indicated proteins by western blotting. H, Heatmap of RNA sequencing analysis of THP-1 derived macrophages treated with either DMSO or 10 μmol L^{-1} LicoD, in the present or absent of 2 μmol L^{-1} cGAMP for 6 h. I, Compared to cGAMP alone, GSEA revealed the downregulated signatures in THP-1 derived macrophages treated with the combination of cGAMP and LicoD. The data represent three independent experiments, with error bars indicating standard deviation (SD) around the mean. A two-tailed unpaired *t*-test was used to analyze significant differences between groups (***, $P<0.001$; **, $P<0.01$; ns, no statistical difference, $P>0.05$).

https://doi.org/10.1007/s11427-024-2703-6

LicoD disrupts STING oligomerization through covalent modification of Cys148

Considering LicoD's broad-spectrum inhibition of signals induced by various STING agonists, including cGAMP, ADU-S100, diABZI, and SR-717, we postulated that LicoD might competitively bind to the ligand-binding pocket with these agonists. To evaluate the ligand-pocket binding affinity, we established a fluorescence polarization assay using FAM-labeled diABZI. Ligands such as SR-717, binding within the pocket, dose-dependently displaced FAM-diABZI from the STING protein (Figure 3A). However, LicoD did not affect the interaction between FAM-diABZI and STING (Figure 3A). Additionally, we introduced mutations in residues involved in the pocket interaction, including T263A and T267A. These mutations significantly reduced the binding of STING with cGAMP, while having no discernible impact on the interaction with LicoD (Figure S5A in Supporting Information). These results indicated that LicoD did not bind to the ligand-binding pocket of STING, nor did it disrupt the binding of STING agonists to the pocket.

Upon binding to agonists, STING protein undergoes oligomerization, which is necessary for STING signal activation (Ergun et al., 2019). We then tested whether LicoD could influence the aggregation of the purified STING protein using size-exclusion chromatography. As shown in Figure 3B, cGAMP can induce STING aggregation, and the addition of LicoD eliminated the cGAMP-induced STING oligomers. LicoD also dose-dependently inhibited the cGAMP-induced STING oligomerization in THP-1 derived macrophages (Figure 3C). Previous studies have reported that the oligomerization and activation of STING require the formation of Cys148-mediated disulfide bridges (Ergun et al., 2019; Humphries et al., 2023). Therefore, we investigated whether LicoD covalently modified Cys148. Mass spectrometry results showed that LicoD can covalently bind to STING, but not to the STING (C148S) variant (Figure 3D). The tandem mass spectrometry identified the peptide [PAEISAVC(C21H22O5)EK] modified by LicoD at Cys148 (Figure 3E). Based on the mass increment after LicoD treatment, the proposed mechanism of action involves Michael addition (Figure S5B in Supporting Information). In summary, these results strongly indicate that LicoD disrupts STING oligomerization through covalent modification of Cys148.

The activation of STING involves translocation from the endoplasmic reticulum to the Golgi apparatus (Ishikawa et al., 2009). Moreover, upon STING oligomerization, TBK1 is recruited to phosphorylate IRF3 and NF-κB, which then initiates downstream gene transcription following their translocation to the nucleus (Hopfner and Hornung, 2020). Immunofluorescence experiments showed that LicoD inhibited the trafficking of STING from the endoplasmic reticulum to the Golgi apparatus by binding to Cys148 of STING (Figure S6 in Supporting Information). In addition, it was found that LicoD disrupted the interaction between STING and TBK1, as well as their co-localization in cells (Figure 3F and G). Additionally, LicoD inhibited the nuclear translocation of IRF3 and NF-κB induced by cGAMP (Figure 3H and I). Some STING variants, such as S154 and M155, have been reported to cause sustained spontaneous activation of STING signaling, leading to a chronic inflammatory disease known as STING-associated vasculopathy with onset in infancy (SAVI) (Liu et al., 2014). We then assessed the inhibitory activity of LicoD against these variants. LicoD significantly inhibited the activation of the S154 variant and demonstrated inhibitory effects on the M155 variant (Figure 3J). This suggests the therapeutic potential of LicoD in diseases associated with STING self-activating mutations.

LicoD attenuates the autoinflammatory phenotype in *Trex1*$^{-/-}$ mice

We next investigated whether LicoD could inhibit the activation of the STING signaling pathway *in vivo*. As depicted in the Figure 4A, pretreatment with LicoD significantly reduced the upregulation of IFN-β and IL-6 in the serum of C57BL/6J mice triggered by diABZI. Additionally, the potential acute toxicity of LicoD was evaluated in C57BL/6J mice via intraperitoneal administration once daily for a duration of 7 days. Notably, no indications of body weight loss or toxic manifestations were observed in mice administered a dosage of 20 mg kg^{-1} (Figure S7A in Supporting Information). These findings suggest the effectiveness and safety of LicoD *in vivo*.

To evaluate the efficacy of LicoD in treating autoinflammatory diseases *in vivo*, we assessed its potential to ameliorate the inflammatory phenotype in *Trex1*$^{-/-}$ mice. *Trex1*$^{-/-}$ mice exhibit severe inflammation in multiple organs, caused by continuous activation of STING signaling due to the accumulation of self-DNA in the cytosol (Gall et al., 2012; Gao et al., 2015; Stetson et al., 2008). In bone marrow-derived macrophages (BMDMs) isolated from *Trex1*$^{-/-}$ mice, LicoD treatment significantly reduced the upregulation of type I IFN and pro-inflammatory cytokines, including *Ifnb1*, *Cxcl10*, *Il6*, *Tnf*, and *Isg15* (Figure 4B; Figure S7B in Supporting Information). To test the therapeutic effect of LicoD in *Trex1*$^{-/-}$ mice, intraperitoneal injection of LicoD was administered every other day for a period of 20 days in both WT and *Trex1*$^{-/-}$ mice. The results demonstrated a notable reduction in the autoinflammatory response in *Trex1*$^{-/-}$ mice upon treatment with LicoD. This was evident through decreased expression levels of type I IFN and pro-inflammatory cytokines (*Ifnb1*, *Cxcl10*, *Il6*, *Tnf*, *Isg15*, and *Isg56*) and diminished inflammatory symptoms in the heart, tongue, stomach, and muscles (Figure 4C and D). Furthermore, the flow cytometry analysis on T cells derived from the spleens revealed that while LicoD did not affect the overall populations of CD8$^+$ T cells, it significantly reduced the frequency of memory CD8$^+$ T cells (CD8$^+$ CD44$^+$ CD62L$^+$) and active CD8$^+$ T cells (CD8$^+$ CD69$^+$) in *Trex1*$^{-/-}$ mice (Figure S7C in Supporting Information). Collectively, these findings strongly indicate that LicoD markedly attenuates the autoinflammatory phenotype in *Trex1*$^{-/-}$ mice.

LicoD alleviates DSS-induced colitis and AOM/DSS-induced CAC in mice

Inflammatory bowel diseases (IBDs), including Crohn's disease and ulcerative colitis, are chronic inflammatory conditions affecting the gastrointestinal tract (Seyedian et al., 2019). Individuals with IBD are at an increased risk of developing colorectal cancer (Nadeem et al., 2020). STING plays a crucial role in maintaining gastrointestinal tract homeostasis and contributes to the pathogenesis of IBDs (Wottawa et al., 2021). Activation of cGAS-STING pathway, induced by commensal bacteria and exosomal dsDNA, leads to intestinal inflammation (Ahn et al., 2017; Zhao et al., 2021). Additionally, accumulation of STING protein in intestinal myeloid cells, noted in mice with

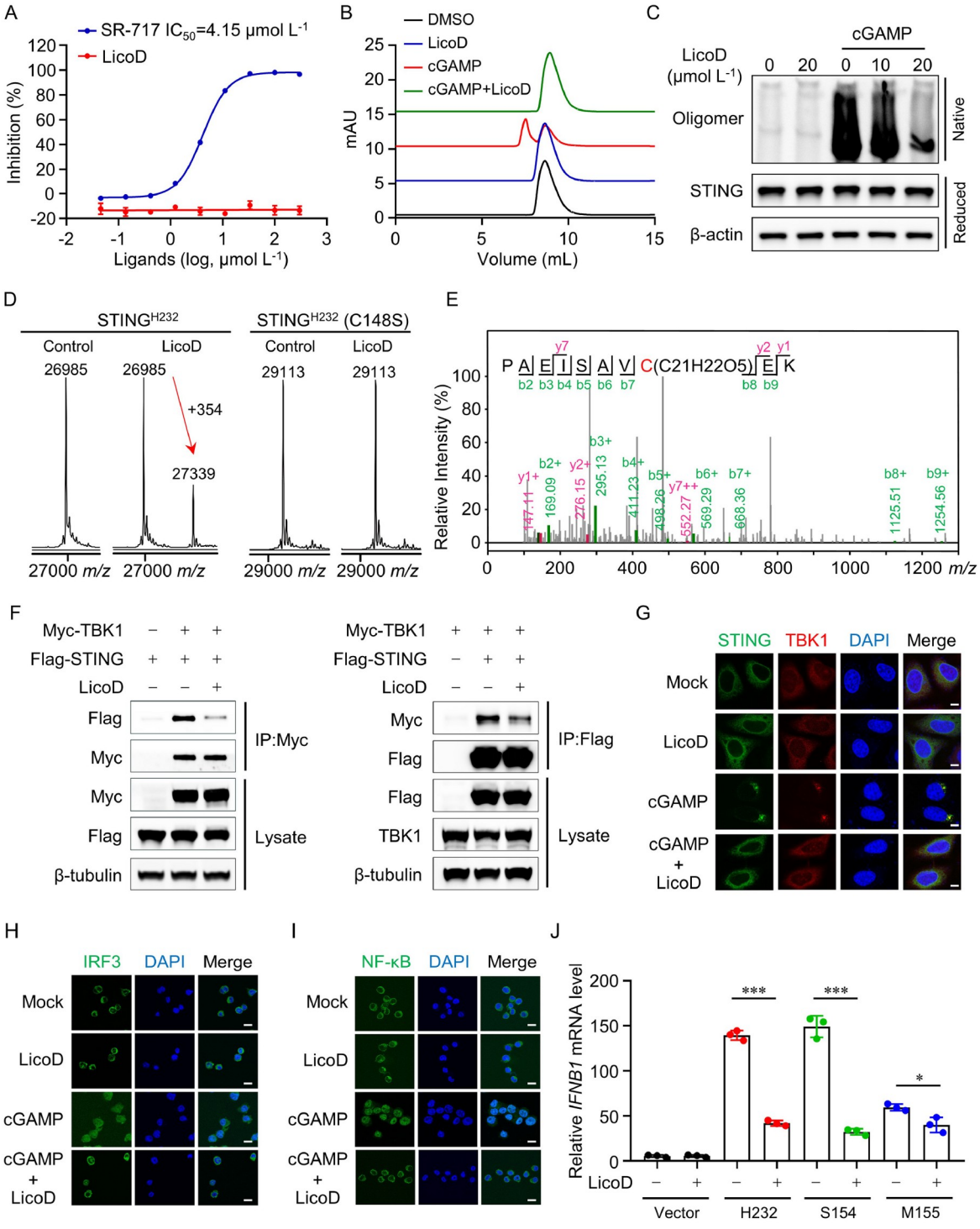

Figure 3. LicoD disrupts STING oligomerization through covalent modification of Cys148. A, LicoD did not displace FAM-diABZI from the STING^{H232} protein in a fluorescence polarization competition assay. SR-717 was served as a positive competitor. B, Size-exclusion chromatogram of 10 μmol L^{-1} purified hSTING^{H232} incubated with 20 μmol L^{-1} LicoD, 100 μmol L^{-1} cGAMP, or a combination of both at 4°C overnight. C, THP-1 derived macrophages were pretreated with the indicated concentration of LicoD for 1 h, followed by stimulation with 2 μmol L^{-1} cGAMP for an additional 2 h. STING oligomerization was analyzed by western blotting. D, Deconvoluted mass spectra for STING^{H232} and STING^{H232} (C148S) protein incubated with or without LicoD. E, Extracted fragment ion chromatogram for the peptide PAEISAVC(C21H22O5)EK from LicoD-treated STING^{H232} protein. F, 293T cells were transfected with Flag-STING and Myc-TBK1 plasmids for 24 h, and subsequently treated with 10 μmol L^{-1} LicoD and 2 μmol L^{-1} cGAMP for 6 h. The effect of LicoD on the interaction between STING and TBK1 was detected by immunoprecipitation assay. G, STING-overexpressing HeLa cells were incubated with 10 μmol L^{-1} LicoD and 2 μmol L^{-1} cGAMP for 2 h. The localization of STING and TBK1 was detected by immunofluorescence assay. Scale bar, 5 μm. H and I, THP-1-derived macrophages were co-treated with 10 μmol L^{-1} LicoD and 2 μmol L^{-1} cGAMP for 2 h. Immunostaining was conducted using the respective IRF3 (H) and NF-κB (I) antibodies, followed by imaging with confocal microscopy. Scale bar, 10 μm. J, 293T cells were transfected with the indicated hSTING variant plasmids for 24 h, and subsequently treated with 10 μmol L^{-1} LicoD for 6 h. The *IFNB1* mRNA level was measured by RT-qPCR. The data represent three independent experiments, with error bars indicating SD around the mean. A two-tailed unpaired *t*-test was used to analyze significant differences between groups (***, $P<0.001$; *, $P<0.05$).

https://doi.org/10.1007/s11427-024-2703-6

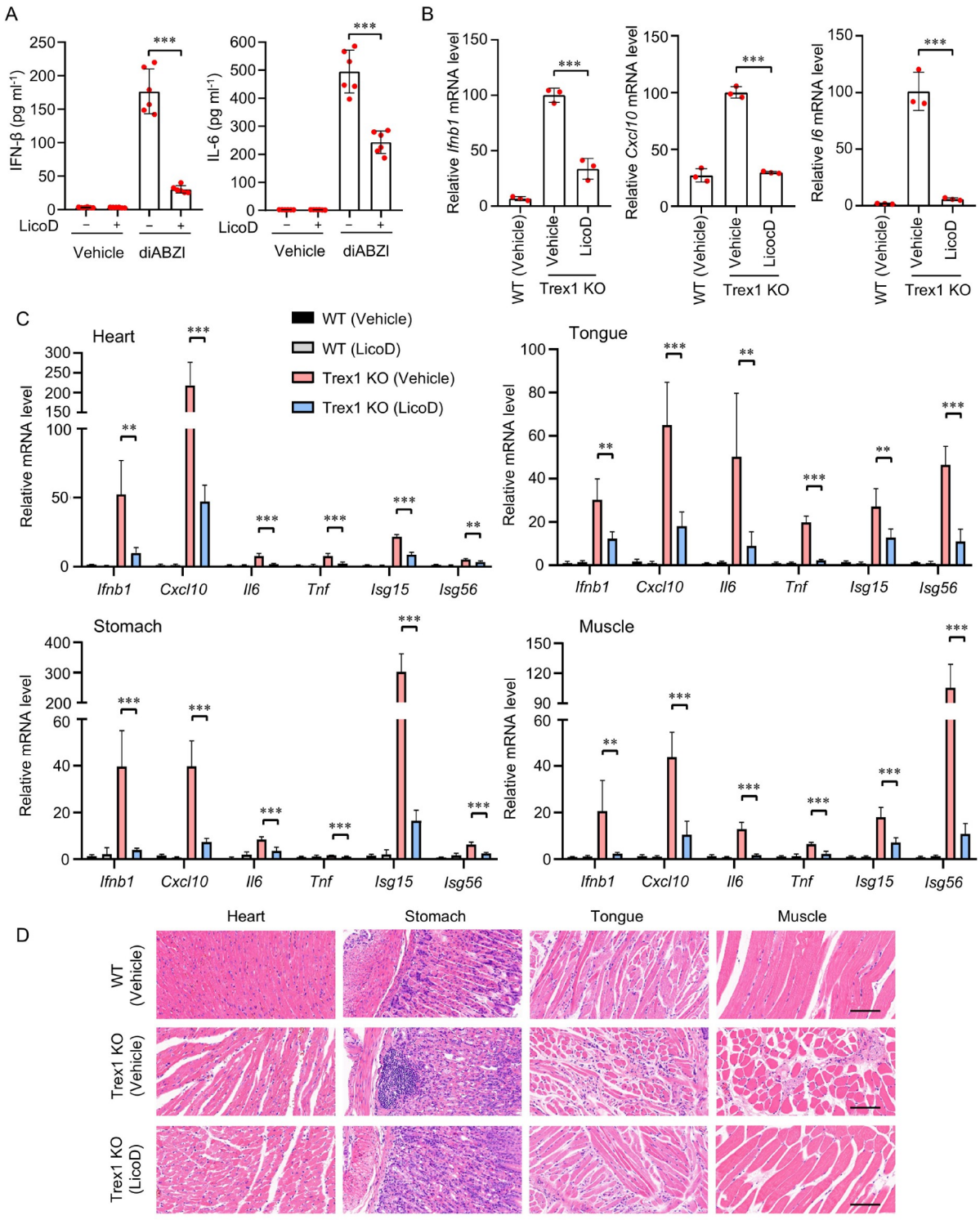

Figure 4. LicoD attenuates the autoinflammatory phenotype in *Trex1*$^{-/-}$ mice. A, C57BL/6J mice were firstly administrated intraperitoneally with LicoD (20 mg kg^{-1}) for 2 h, followed by subcutaneous stimulation with diABZI (2.5 mg kg^{-1}) for another 4 h. The concentrations of IFN-β and IL-6 in the serum were detected (n=6). B, BMDMs derived from WT and *Trex1*$^{-/-}$ mice were treated with LicoD (10 μmol L^{-1}) or DMSO for 24 h, subsequently, the mRNA expression levels of *Ifnb1*, *Cxcl10*, and *Il6* were detected by RT-qPCR. C and D, The WT and *Trex1*$^{-/-}$ mice received intraperitoneal injections of 3 mg kg^{-1} LicoD or vehicle every other day for a duration of 20 days. At the end of the experiment, the mice were euthanized and tissue samples from the heart, tongue, stomach, and muscles were collected for mRNA expression measurement (C) (n=6) and hematoxylin and eosin (H&E) staining analysis (D), scale bar, 100 μm. Error bars represent SD around the mean; two-tailed unpaired t-test was used to analyze significant differences between groups (***, P<0.001; **, P<0.01).

colitis and humans with IBDs, exacerbates the inflammatory phenotype (Shmuel-Galia et al., 2021). Deficiency or inhibition of cGAS-STING signaling has been shown to significantly ameliorate intestinal inflammation (Ahn et al., 2017; Song et al., 2023;

Wang et al., 2021). Consequently, we investigated whether LicoD could be used to treat colitis and colitis-associated colon cancer (CAC) in mice.

The mice were fed with water containing 3% dextran sodium sulfate (DSS) for 7 days to induce colitis, while simultaneously receiving intraperitoneal administration of either 20 mg kg^{-1} of LicoD or vehicle (Figure 5A). The group of mice fed with water containing DSS experienced a significant decline in body weight, while administration of LicoD effectively mitigated this weight loss progression (Figure 5B). Reduction in colon length, a characteristic feature of DSS-induced colitis in mice, was significantly prevented by LicoD administration (Figure 5C and D). Analysis of histological staining sections revealed that LicoD mitigated DSS-induced inflammatory cell infiltration, epithelial cell injury, crypt swelling, and destruction in colon sections (Figure 5E). Furthermore, LicoD significantly reduced the histological score associated with acute colitis (Figure 5F). Additionally, mice fed with water containing DSS showed elevated expression levels of *Il6*, *Il1b*, and *Tnf* mRNA in colorectal tissues, along with increased concentrations of IL-6, IL-1β, and TNF in the serum. LicoD administration significantly reduced the expression of these cytokines (Figure 5G and H). Of note, feeding with DSS indeed resulted in the activation of STING signaling, as evidenced by increased phosphorylation of STING, TBK1, and RF3 proteins in colorectal tissues. Treatment with LicoD was found to effectively reduce the phosphorylation levels of these proteins (Figure S8 in Supporting Information). In summary, LicoD exhibits a substantial therapeutic impact on DSS-induced colitis in mice.

Considering that LicoD significantly alleviated the inflammatory responses in the colon of mice with DSS-induced colitis, it's therapeutic effect on CAC was then investigated. CAC mouse model was established by administering azoxymethane (AOM) on day 0 and periodic DSS treatment. LicoD was intraperitoneally injected into the mice once every 2 days, beginning with the start of the second cycle (Figure 6A). At the end of the study, mice were euthanized, and colon tissues were collected for tumor growth analysis. As shown in Figure 6B–D, LicoD treatment significantly inhibited the occurrence and growth of AOM/DSS-induced tumors in a dose-dependent manner. Moreover, LicoD treatment resulted in a substantial reduction in inflammatory indicators within colon tissues, including diminished inflammatory manifestations and cytokines expression (Figure 6E; Figure S9A in Supporting Information). Additionally, the concentrations of IL-6, IL-1β, and TNF in the serum decreased following LicoD treatment compared to the vehicle group (Figure S9B in Supporting Information). Importantly, LicoD treatment reduced AOM/DSS-induced phosphorylation levels of STING, TBK1, IRF3, NF-κB, and STAT3 in colon tissues (Figure 6F), suggesting that LicoD exerts anti-CAC effects by inhibiting cGAS-STING signaling. Notably, AOM/DSS treatment elevated the expression of Ki-67, a widely recognized biomarker of cellular proliferation (Sun and Kaufman, 2018), in the intestinal epithelium. Following LicoD intervention, a notable reduction in Ki-67 expression was observed (Figure 6F). Collectively, these findings demonstrate that LicoD can prevent CAC by inhibiting STING-mediated inflammatory responses.

DISCUSSION

The aberrant activation of STING signaling is implicated in several autoimmune and inflammatory disorders (Hopfner and Hornung, 2020), rendering the targeted suppression of STING a promising therapeutic strategy for these conditions. However, the development of effective STING inhibitors has not yielded satisfactory results. The STING dimer's two ligand-binding domains form a ligand-binding pocket, which serves as the binding site for known STING inhibitors, such as SN-011 and Astin C, as well as for the majority of known STING agonists (Decout et al., 2021). This pocket is highly polar and undergoes pronounced conformational changes during the activation process (Shang et al., 2019), factors that limit the discovery of STING inhibitors based on docking approaches. Furthermore, the discovery of STING inhibitors based on cellular phenotypes proves time-consuming and labor-intensive, and challenging in ensuring specificity.

In this study, a protein primary sequence-based and binding site-independent TransformerCPI model was utilized to discover compounds capable of binding to STING protein. The natural product LicoD was identified as a potent and selective STING inhibitor. LicoD effectively inhibited STING-mediated *IFNB1* expression without affecting the signaling mediated by cGAS, TBK1, or IRF3. Importantly, LicoD did not suppressed the expression of *IFNB1* and *TNF* mRNA triggered by TLR3/4 pathway activation. Furthermore, LicoD treatment significantly reduced the expression of inflammatory cytokines in *Trex1*$^{-/-}$ BMDMs and ameliorated the inflammatory phenotype in *Trex1*$^{-/-}$ mice. In mouse models of DSS-induced colitis and AOM/DSS-induced colitis-associated colon cancer, LicoD alleviated intestinal inflammation by inhibiting the activation of STING signaling. LicoD, a key component extracted from the licorice root, has exhibited notable anti-inflammatory properties (Yang et al., 2017b). Our study suggested that the anti-inflammatory efficacy of licorice can be partially ascribed to the inhibition of STING signaling activation by LicoD.

Mechanically, LicoD did not bind within the ligand-binding pocket but covalently modified STING at cysteine 148. This modification impeded STING oligomerization, thereby inhibiting the recruitment of TBK1 and the nuclear translocation of IRF3 and NF-κB. As a result, LicoD can suppress not only agonist-mediated STING signal activation but also ligand-independent autoactivation of STING variants. Of note, Cys148 is located in the flexible linker region, which connects the ligand-binding domain to the transmembrane domain and lacks a distinct pocket, rendering traditional structure-based screening methods ineffective for discovering LicoD.

In conclusion, this study unveils the therapeutic potential of LicoD in the treatment of STING-driven inflammatory diseases. Furthermore, it showcases the effectiveness of the TransformerCPI model in identifying allosteric compounds beyond the traditional binding sites.

MATERIALS AND METHODS

Reagents

LicoD (HY-N4187), cGAMP (HY-100564A), diABZI (HY-112921B), ADU-S100 (HY-12885A), SR-717 (HY-131454), lipopolysaccharide (LPS) (HY-D1056), Pam3CSK4 (HY-P1180), IL-1β (HY-P7028) and Zymosan A (HY-W250113) were purchased from MedChemExpress (MCE). The solvent PEG400 (S6705) was from Selleck, and dextran sulfate sodium (DSS)

https://doi.org/10.1007/s11427-024-2703-6

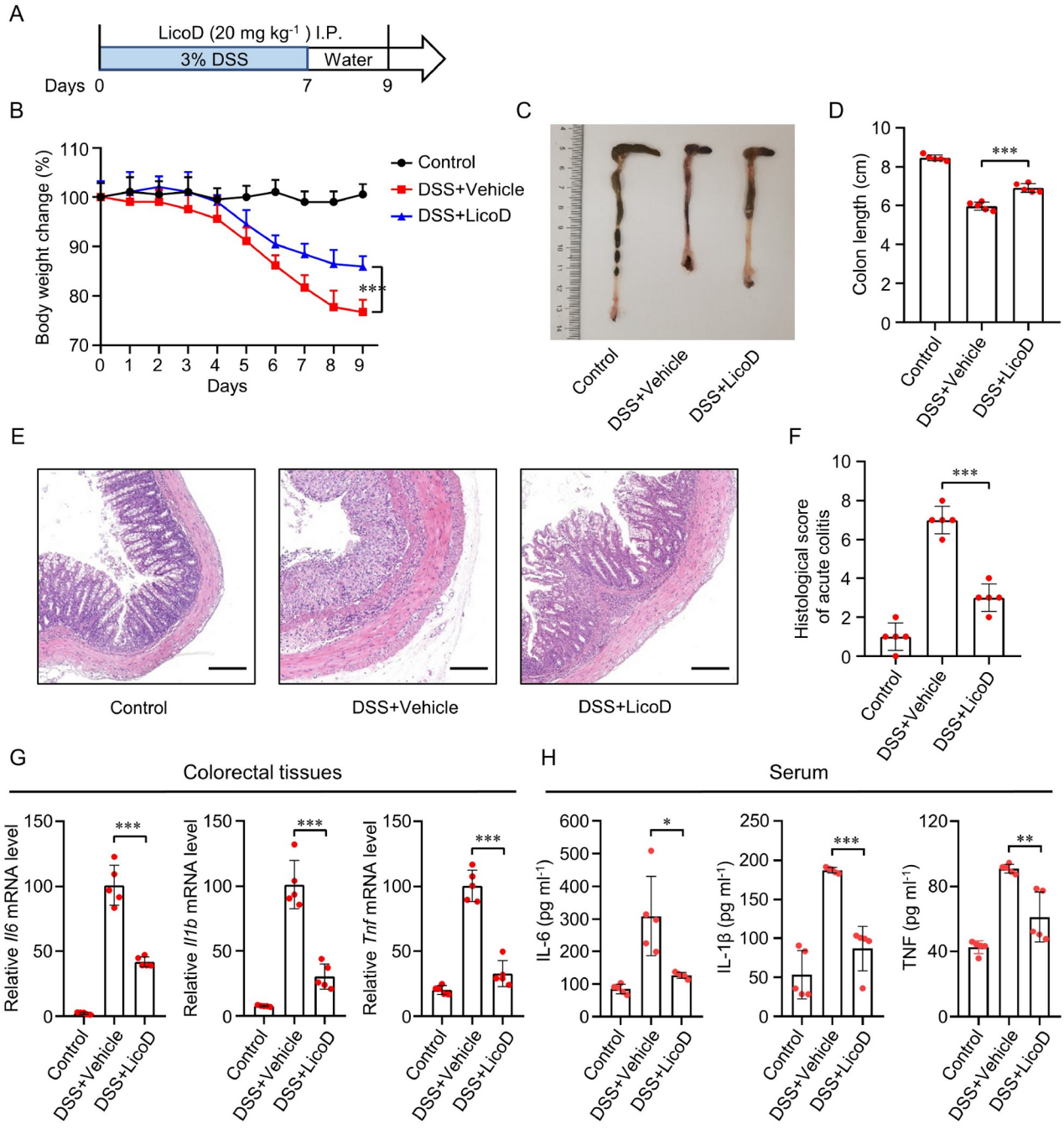

Figure 5. LicoD alleviates DSS-induced colitis in mice. A, The schematic of DSS-induced colitis mouse model. B, Weight loss of mice was measured daily and expressed as the percentage of initial body weight (n=5). C and D, Length of colons from mice was measured at the end of the study (n=5). E and F, Representative H&E-stained images of mouse colorectal tissues and colonic inflammation scores at the end of the study (n=5), scale bar, 200 μm. G, The transcription levels of *Il6*, *Il1b*, and *Tnf* in colorectal tissues of mice were detected by RT-qPCR (n=5). H, The concentrations of IL-6, IL-1β, and TNF in the serum of mice were determined by ELISA assay (n=5). Error bars represent SD around the mean; a two-tailed unpaired t-test was used to analyze significant differences between groups (***, P<0.001; **, P<0.01; *, P<0.05).

(216011090) was provided by MPbio. Azoxymethane (AOM) (A169090) was purchased from Aladdin.

Plasmids and transfection

Flag-STING, Flag-STING^{C148S}, Myc-TBK1 and IRF3-5D plasmids were constructed using SnapGene and subsequently synthesized by Synbio Technologies. Double-stranded DNA (dsDNA) such as G3-ended Y-form Short DNA (G3-YSD) (InvivoGen, tlrl-ydna) and Interferon Stimulatory DNA (ISD) (InvivoGen, tlrl-isdn), Flag-STING, Flag-STING^{C148S}, Myc-TBK1, and IRF3-5D plasmids were transfected with PolyJet (SignaGen, SL100688). Transfection of poly(I:C) (InvivoGen, tlrl-picw) was performed with Lipofectamine 2000 (Invitrogen, 11668019) according to the manufacturer's instructions. All constructs were verified by standard sequencing.

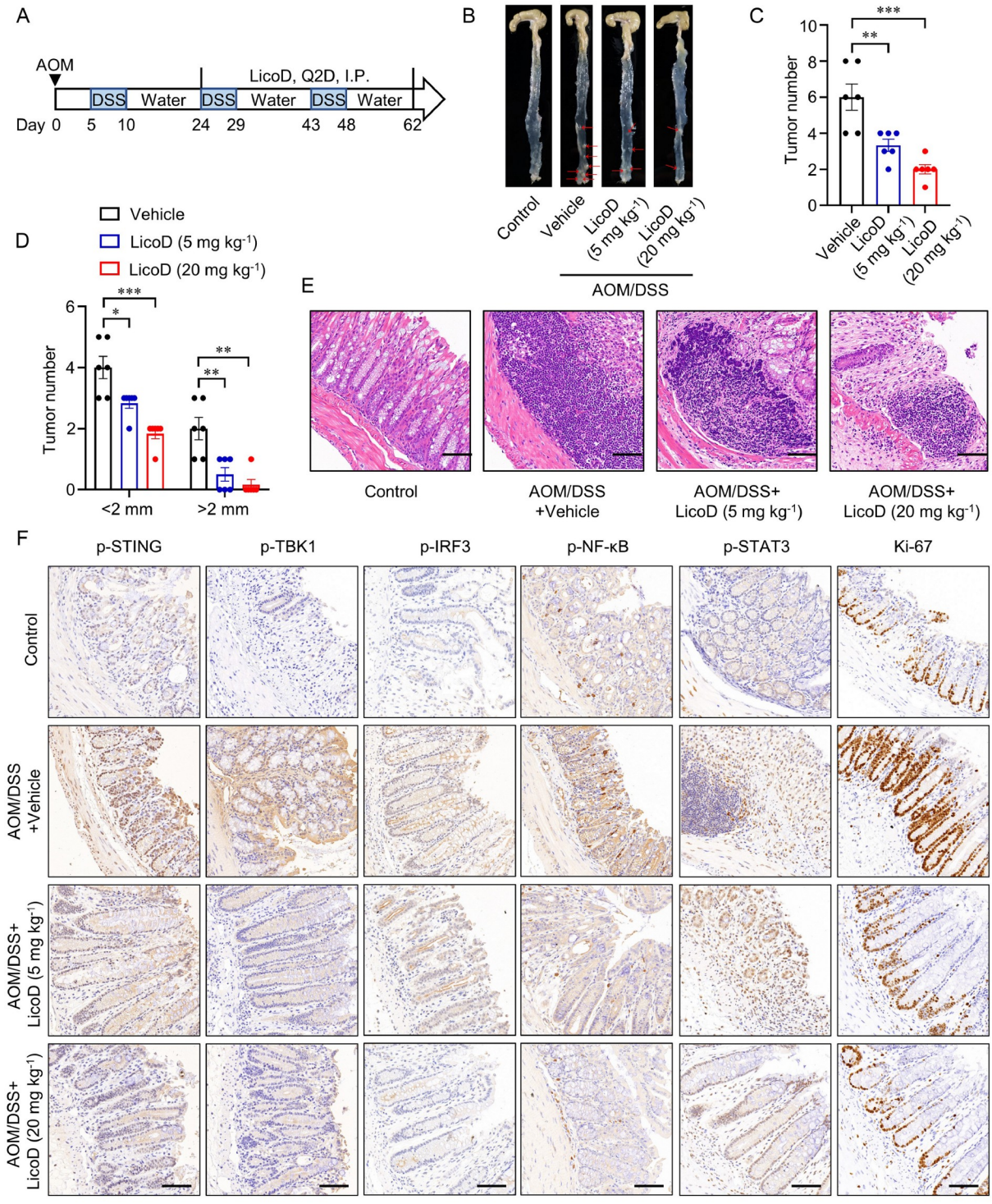

Figure 6. LicoD alleviates AOM/DSS-induced CAC in mice. A, The schematic of AOM/DSS-induced CAC mouse model. C57BL/6J mice were intraperitoneally administered 8 mg kg^{-1} of AOM on day 0, followed by a 2% DSS solution for 5 days starting on day 5, and then regular drinking water for 2 weeks. This cycle was repeated twice. B, Representative images of colon tumor development in mice with AOM/DSS-induced CAC. Arrows indicate tumors. C and D, The effect of LicoD on the tumor number (C) and tumor size (D) in mice with AOM/DSS-induced CAC (n=6). E, Representative H&E-stained images of mouse colon tissues, scale bar, 100 μm. F, The colon tissues of mice were stained with antibodies against p-STING, p-TBK1, p-IRF3, p-NF-κB, p-STAT3, and Ki-67, representative images were shown, scale bar, 100 μm. Error bars represent SD around the mean; a two-tailed unpaired t-test was used to analyze significant differences between groups (***, P<0.001; **, P<0.01; *, P<0.05).

Cell lines

Human myeloid leukemia mononuclear cells (THP-1), mouse macrophage cell line (RAW264.7), 293T and HeLa cells were purchased from the American Type Culture Collection (ATCC). THP1-Blue ISG cells and RAW-Lucia ISG cells were purchased from InvivoGen. RAW264.7 cells, 293T and HeLa cells were cultured in DMEM medium (BasalMedia, L110KJ) supplemented

https://doi.org/10.1007/s11427-024-2703-6

with 10% fetal bovine serum (FBS, Gibco, 10099141C) and 1% Penicillin-Streptomycin (PS, Gibco, 15140122). THP-1 cells were cultured in RPMI-1640 medium (BasalMedia, L210KJ) with the same supplement. THP-1 derived macrophages were differentiated from THP-1 cells incubated with phorbol-12-myristate-13-acetate (PMA, 100 ng mL^{-1}). Bone marrow-derived macrophages (BMDMs) were obtained by induced differentiation of bone marrow cells in the presence of M-CSF (PeproTech, 20 ng mL^{-1}) and maintained in growth media consisting of DMEM medium with 10% FBS and 1% PS. All cells were incubated at 37°C under a 5% (v/v) CO_2 atmosphere.

Sequence-based AI screening methods

In order to quickly discover small-molecule compounds targeting STING, the optimized TransformerCPI model was used for virtual screening of small-molecule compounds targeting STING protein (Chen et al., 2020). The amino acid sequence of STING (Uniprot ID: Q86WV6) was input. AI scoring, ranking and screening were performed on the SPECS library and the compound library built by the laboratory. The top 1,000 compounds were clustered into 100 groups. Within each group, the compound with the highest predicted score was selected as the representative molecule for experimental evaluation.

Protein expression and purification

The gene sequence encoding carboxy-terminal domain (CTD, residues 139–379) of human STING (hSTING^{H232}, hSTING^{R232}, hSTING^{S154} and hSTING^{M155}) and murine STING CTD (residues 139–372) were inserted into a modified pET-28a vector with 6×His-SUMO tag. The gene sequence encoding hSTING^{C148S} CTD was directly inserted into pET-28a vector. All proteins were expressed in *Escherichia coli* BL21 (DE3) competent cells. The cells were grown in Luria-Bertani (LB) medium at 37°C for 4 h and induced with 0.2 mmol L^{-1} isopropyl β-D-1-thiogalactopyranoside (IPTG) overnight at 16°C. The cells were harvested and lysed in buffer (20 mmol L^{-1} HEPES (pH 7.4), 200 mmol L^{-1} NaCl, 10 mmol L^{-1} imidazole, 1 mmol L^{-1} TCEP). After centrifugation, the supernatant was initially purified on HisTrap FF columns (GE Healthcare). The SUMO tag was cleaved by SUMO-specific proteases (ULP1) overnight. Further purification was conducted on a Superdex 75 10/300 GL column (GE Healthcare) with STING buffer (20 mmol L^{-1} HEPES (pH 7.4), 200 mmol L^{-1} NaCl). The purified proteins were concentrated and stored at –80°C.

Protein thermal shift (PTS) assay

The thermostability of STING protein was measured by CFX96 Real-Time PCR Detection System (Bio-Rad). STING protein and 5× SYPRO Orange were diluted to 19 μL with STING buffer. Subsequently, LicoD was added to a reaction system of 20 μL to be tested. The fluorescence signal was monitored and collected at 25–90°C, and the T_m values of STING were determined using protein thermal migration software (Bio-Rad).

Surface plasmon resonance (SPR) assay

SPR binding assays were performed using Biacore T200 and Biacore 8K instrument (GE Healthcare) with running buffer HBS-EP (10 mmol L^{-1} HEPES (pH 7.4), 150 mmol L^{-1} NaCl). Purified STING protein was immobilized onto on the sensor chip CM5 using standard amino-coupling methods in 10 mmol L^{-1} sodium acetate (pH 4.0). LicoD in a series of two-fold dilutions was flowed through the sensor chip at a flow rate of 30 Ml min^{-1} for kinetic assays. The contact time was 120 s and the dissociation time was 180 s. The equilibrium dissociation constant (K_D) values were fitted using Biacore T200 or Biacore 8K Evaluation software.

Isothermal titration calorimetry (ITC) assay

The binding of STING and LicoD was determined by isothermal titration microcalorimeter MicroCal PEAQ-ITC. All solutions were performed in a buffer of 20 mmol L^{-1} HEPES (pH 7.4), 200 mmol L^{-1} NaCl at 25°C. The STING^{H232} was placed in the sample chamber, and LicoD was added with a syringe in twenty consecutive additions of 2 μL (with an initial injection of 0.4 μL). Data was analyzed using MicroCal PEAQ-ITC Analysis Software.

Cytotoxicity assay

Cell viability was determined using the CellTiter-Glo luminescent cell viability assay (Promega, G7572) according to the manufacturer's instruction, and the luminescent signal was detected by a Spark microplate reader (TECAN).

SEAP reporter assay

THP1-Blue ISG cells were plated in 96-well plates and cultured overnight. The cells were treated with cGAMP and a series of serial dilutions of LicoD. After 24 h, SEAP activity was measured with the Quanti-Blue Kit (InvivoGen) according to the respective manufacturer's instructions.

Luciferase reporter assay

RAW-Lucia ISG cells were plated in 96-well plates and cultured overnight. The cells were treated with cGAMP and a series of serial dilutions of LicoD. After 24 h, Luciferase activity was tested with the Quanti-Luc Kit (InvivoGen) according to the respective manufacturer's instructions.

RNA sequencing

THP-1 derived macrophages were treated with LicoD (10 μmol L^{-1}) or DMSO in the present or absent of cGAMP (2 μmol L^{-1}) for 6 h. The total RNA in the cells was extracted by RNA extraction reagent (Vazyme, R401-01). Subsequent sample quality inspection, RNA sequencing and differential gene expression analysis were completed by Majorbio. Differential gene set enrichment analysis was performed with Gene Set Enrichment Analysis (GSEA).

Western blot

Cells or tissue were harvested and lysed in RIPA Lysis Buffer (Beyotime, P0013C) containing protease inhibitor (Bimake, B14001) and phosphatase inhibitor (Bimake, B15001). Protein concentrations were determined by the BCA Protein Assay Kit (Thermo Fisher, 23225). The samples were prepared using SDS-PAGE Sample Loading Buffer (Beyotime, P0015L). Proteins were

separated by sodium dodecyl sulfate-polyacrylamide gel electrophoresis (SDS-PAGE) and transferred onto nitrocellulose (NC) membranes. The NC membranes were blocked with 5% skim milk and incubated with primary antibodies overnight at 4°C. The horseradish peroxidase (HRP)-conjugated anti-Rabbit IgG (H+L) (Promega, W4011) was used as secondary antibody at room temperature (RT) for 2 h. Finally, the protein banding on membranes were detected with ECL kit (Meilunbio, MA0186) and visualized by the GeneGnome XRQ NPC. The following primary antibodies were used: anti-pSTING (human, 50907S), anti-pSTING (mouse, 72971S), anti-STING (13647S), anti-pTBK1 (5483S), anti-TBK1 (3504s), anti-pIRF3 (29047S), anti-IRF3 (4302S), anti-pNF-κB p65 (3033S), anti-NF-κB p65 (8242S), anti-pSTAT3 (9145S), anti-STAT3 (30835S), β-Tubulin (15115S) were purchased from Cell Signaling Technology (CST).

Real-time quantitative PCR (RT-qPCR)

Total RNA was extracted with RNA-easy Isolation Reagent (Vazyme, R701-01) following the manufacturer's instructions. The quantified RNA was reverse transcribed into cDNA using HiScript II Q RT SuperMix II (Vazyme, R223-01). RT-qPCR was performed using the ChamQ SYBR qPCR Master Mix (Vazyme, Q331-02) in a CFX96TM Real-Time PCR Detection System (Bio-Rad). All PCR primers used are shown in Table S2 in Supporting Information.

Immunofluorescence microscopy

THP-1 derived macrophages, HeLa and 293T cells were fixed with 4% paraformaldehyde fixative for 30 min, permeabilized in Triton X-100 for 30 min and blocked using 5% bovine serum Albumin (BSA) for 30 min at RT. Cells were stained with primary antibodies diluted with Triton X-100 and BSA (1:2) at 4°C overnight and fluorescent-conjugated secondary antibody for 45 min at RT. The nuclei were stained with anti-fluorescence quenching sealing solution (including DAPI) (Beyotime, P0131) for 10 min. Finally, images were captured using a confocal microscope (Leica). The antibodies were used as follows: anti-IRF3 (CST, 11904S), anti-NF-κB p65 (CST, 8242S), anti-TBK1 (Abcam, ab40676), anti-STING (Invitrogen, MA5-26030), Anti-GM130 (Abcam, ab52649), Alexa Flour™ 488 Goat anti-Mouse IgG (Invitrogen, A11029), Alexa Flour™ 488 Goat anti-Rabbit SFX Kit (Invitrogen, A11034), Alexa Flour™ 633 Goat anti-Rabbit IgG (H+L) (Invitrogen, A21071).

Fluorescence polarization (FP) assay

For compound competition binding assay, 5-FAM labeled diABZI was used as a tracer (Shan et al., 2023). The assay was performed in black 384-well microplates containing 40 μL reaction system. The diluted LicoD and 400 nmol L^{-1} STING proteins was incubated for 30 min at RT and then the tracer was added to the reaction mixture. After 30 min, the FP values were measured on a Spark microplate reader (TECAN) using wavelengths of 485 nm for excitation and 535 nm for emission.

Size-exclusion chromatography

The size-exclusion chromatography was conducted to determinate the molecular weight of STING protein. The purified STING proteins (5 μmol L^{-1}) and LicoD (20 μmol L^{-1}) were incubated with and without cGAMP (100 μmol L^{-1}) at RT overnight. Subsequently, the proteins were analyzed using size-exclusion chromatography (Superdex 75 Increase 10/300 GL) on an ÄKTA chromatography system (GE Healthcare).

Analyses of STING oligomerization by native gels

Native gel analysis for STING oligomerization assay was carried out as described previously (Iwamura et al., 2001). The THP-1 derived macrophages were lysed in NP-40 lysis buffer and quantified using BCA Protein Assay Kit. Equal amounts of total proteins were treated with Native Gel Sample Loading Buffer and run on a Native-PAGE gel. Proteins were transferred to the NC membranes. Subsequent steps were performed according to Western blot protocol.

Mass spectrometry

The diluted LicoD (500 μmol L^{-1}) and STING proteins (50 μmol L^{-1}) were incubated at 4°C overnight. The protein molecular weights were determined by Q Exactive (Thermo) and 6545 XT (Aglient) mass spectrometer. To identify compound binding sites, proteins were digested with trypsin (10 ng μL^{-1}) at 37°C for 17 h. The following day, the resulting supernatant was subjected to lyophilization, desalination, and re-lyophilization. This was followed by the addition of a 0.1% formic acid (FA) solution to reconstitute the peptide lyophilized powder. After further centrifugation, the supernatant underwent mass spectrometric analysis using Q-Exactive. Mass spectrometry data were processed using MaxQuant software (version 1.6.5.0). The false discovery rate (FDR) for peptides and proteins was controlled <1% by Andromeda search engine.

Co-immunoprecipitation (Co-IP)

To determine the formation of STING-TBK1 complex in cells, Flag-STING and Myc-TBK1 plasmids were transfected into 293T cells. Cells were co-treated with cGAMP (2 μmol L^{-1}) and LicoD (10 μmol L^{-1}) for 6 h and lysed in a Western and IP lysate (Beyotime, P0013J) containing protease inhibitor and phosphatase inhibitor. Protein in the lysates were quantified by the BCA Kit. Cleared supernatants were immunoprecipitated with Anti-Flag or Anti-Myc agarose beads (Bimake) at RT for 2 h. The beads were washed at least three times with PBST buffer (NaCl 136 mmol L^{-1}, KCl 2.65 mmol L^{-1}, Na_2HPO_4 8 mmol L^{-1}, KH_2PO_4 1.75 mmol L^{-1}, 0.5% Tween 20) and denaturalized with SDS-PAGE Sample Loading Buffer by boiling for 5 min. The immunoprecipitation samples were detected and analyzed by Western blotting. Primary and secondary antibodies used were as follows: DYKDDDDK Tag (anti-Flag Tag, 14793S), anti-Myc Tag (2278S) were purchased from CST. HRP-conjugated anti-Rabbit IgG (H+L) (W4011) was purchased from Promega.

Mice and *in vivo* studies

The mice used in the experiments were wild-type (WT), *Trex1*$^{+/-}$ and *Trex1*$^{-/-}$ C57BL/6J mice. WT mice were purchased from Beijing Huafukang Biotechnology and *Trex1*$^{+/-}$ mice were kindly provided by Xiao Yichuan's group (Shanghai Institute of

https://doi.org/10.1007/s11427-024-2703-6

Nutrition and Health, Chinese Academy of Sciences). *Trex1*$^{-/-}$ mice were generated by further mating the male and female *Trex1*$^{+/-}$ mice. The genotyping of these mice was performed using Quick Genotyping Assay Kit for Mouse Tail (Beyotime, D7283M) with primers *Oam878* and *Oge514*. All animal experiments were performed in strict accordance with the guidelines of the Institutional Animal Care and Use Committees (IACUC) of the Shanghai Institute of Materia Medica, Chinese Academy of Sciences.

For the evaluation of LicoD's acute toxicity, mice were randomly divided into two groups (n=5) and intraperitoneally injected with DMSO or LicoD (20 mg kg^{-1}) once a day for one week. Body weight was measured every day.

To evaluate the therapeutic effect of LicoD in *Trex1*$^{-/-}$ mice, 6-week-old *Trex1*$^{-/-}$ mice were intraperitoneally injected with LicoD (3 mg kg^{-1}) every other day for 20 days, with WT mice serving as controls. Tissue samples obtained from these mice were analyzed by RT-qPCR, H&E staining, and flow cytometry.

The acute colitis model in mice was established by administering 3% (w/v) DSS (molecular weight 36,000–50,000) in their drinking water for seven consecutive days (Wirtz et al., 2017). LicoD was injected intraperitoneally daily at a dose of 20 mg kg^{-1} for 9 days and mice were weighed daily. Serum and colorectal tissues from these mice were subsequently processed for analysis using ELISA kits, RT-qPCR, and H&E staining.

To establish the experimental model of CAC in C57BL/6J mice, the mice were intraperitoneally administered 8 mg kg^{-1} of AOM on day 0. This was followed by providing a 2% DSS solution for five days starting on day 5, which was then succeeded by regular drinking water for a duration of two weeks (Hu et al., 2021). This cycle was repeated twice. The mice were intraperitoneally injected with either LicoD (5 mg kg^{-1} or 20 mg kg^{-1}) or vehicle every 2 days starting from the 2nd cycle. Finally, mice serum and colorectal tissues were collected for analysis using RT-qPCR, H&E, immunohistochemical (IHC) staining, or ELISA kits.

Flow cytometry

The infiltration of immune cells in mice spleen tissue was analyzed by flow cytometry. The spleens of mice were cut into pieces and filtered through cell filters in PBS. The cells were harvested and resuspended in ammonium chloride solution to remove red blood cells. Subsequently, cells were stained with Fixable Viablity Stain 700 (BD Horizan, 564997) and blocked using FcR closure reagent anti-mouse CD16/32 antibody for 10 min. Blocked cells were incubated with the indicated antibody in PBS containing 2% FBS. Stained cells were centrifuged and resuspended in PBS containing 2% FBS and detected by flow cytometry. Data was collected using a CytoFlex flow cytometer (Beckman) and analyzed using Flowjo software. The antibodies in the Flow Cytometry experiments were used as follows: CD3-FITC (11-0032-82), CD44-APC (17-0441-82), CD62L-PC7 (25-0621-82), CD69-PE (12-0691-82) were purchased from Invitrogen and CD8-BV421 (100738) was provided by Biolegend.

Enzyme linked immunosorbent assay (ELISA)

Concentrations of the cytokines in in the serum of mice were measured by ELISA Kit following the manufacturer's instructions. Mouse IL-6 ELISA Kit (abs520004-96T), Mouse IL-1β ELISA Kit (abs520001-96T), and Mouse TNF ELISA Kit (abs520010-96T) were purchased from Absin. Mouse IFN-beta DuoSet ELISA Kit (DY8234-05) was purchased from R&D Systems.

Statistical analysis

GraphPad Prism 8.0.1 software was used to perform statistical analysis. The statistical significance of the data was analyzed by two-tailed unpaired t-test. Data are presented as mean±SD. The significance levels were set as: ***, P<0.001; **, P<0.01; *, P<0.05; ns, no statistical differences, P>0.05.

Compliance and ethics

The author(s) declare that they have no conflict of interest. All animal experiments were carried out in strict accordance with the guidelines and regulations of the Institutional Animal Care and Use Committees (IACUC) of the Shanghai Institute of Materia Medica, Chinese Academy of Sciences.

Acknowledgement

We thank the staff members of the Large-scale Protein Preparation System at the National Facility for Protein Science in Shanghai (NFPS), Shanghai Advanced Research Institute, Chinese Academy of Science, China for providing technical support and assistance in data collection and analysis. We gratefully acknowledge financial support from National Natural Science Foundation of China (T2225002, 82273855, 82304379, 81903639), National Key Research and Development Program of China (2022YFC3400504), the Youth Innovation Promotion Association CAS (2023296), the SIMM-SHUTCM Traditional Chinese Medicine Innovation Joint Research Program (E2G805H), the open fund of state key laboratory of Pharmaceutical Biotechnology, Nanjing University, China (KF-202301), the Natural Science Foundation of Shanghai (22ZR1474300), Lingang Laboratory (LG202102-01-02, LG-QS-202204-01), and Young Elite Scientists Sponsorship Program by CAST (2023QNRC001)

References

Abe, T., and Barber, G.N. (2014). Cytosolic-DNA-mediated, STING-dependent proinflammatory gene induction necessitates canonical NF-κB activation through TBK1. J Virol 88, 5328–5341.

Ablasser, A., Goldeck, M., Cavlar, T., Deimling, T., Witte, G., Röhl, I., Hopfner, K.P., Ludwig, J., and Hornung, V. (2013). cGAS produces a 2′-5′-linked cyclic dinucleotide second messenger that activates STING. Nature 498, 380–384.

Ahn, J., Ruiz, P., and Barber, G.N. (2014). Intrinsic self-DNA triggers inflammatory disease dependent on STING. J Immunol 193, 4634–4642.

Ahn, J., Son, S., Oliveira, S.C., and Barber, G.N. (2017). STING-dependent signaling underlies IL-10 controlled inflammatory colitis. Cell Rep 21, 3873–3884.

Barber, G.N. (2015). STING: infection, inflammation and cancer. Nat Rev Immunol 15, 760–770.

Chen, L., Tan, X., Wang, D., Zhong, F., Liu, X., Yang, T., Luo, X., Chen, K., Jiang, H., Zheng, M., et al. (2020). TransformerCPI: improving compound–protein interaction prediction by sequence-based deep learning with self-attention mechanism and label reversal experiments. Bioinformatics 36, 4406–4414.

Crow, Y.J., and Manel, N. (2015). Aicardi–Goutières syndrome and the type I interferonopathies. Nat Rev Immunol 15, 429–440.

Decout, A., Katz, J.D., Venkatraman, S., and Ablasser, A. (2021). The cGAS–STING pathway as a therapeutic target in inflammatory diseases. Nat Rev Immunol 21, 548–569.

Ergun, S.L., Fernandez, D., Weiss, T.M., and Li, L. (2019). STING polymer structure reveals mechanisms for activation, hyperactivation, and inhibition. Cell 178, 290–301.e10.

Gall, A., Treuting, P., Elkon, K.B., Loo, Y.M., Gale Jr., M., Barber, G.N., and Stetson, D. B. (2012). Autoimmunity initiates in nonhematopoietic cells and progresses via lymphocytes in an interferon-dependent autoimmune disease. Immunity 36, 120–131.

Gao, D., Li, T., Li, X.D., Chen, X., Li, Q.Z., Wight-Carter, M., and Chen, Z.J. (2015). Activation of cyclic GMP-AMP synthase by self-DNA causes autoimmune diseases. Proc Natl Acad Sci USA 112, E5699–E5705.

Glück, S., Guey, B., Gulen, M.F., Wolter, K., Kang, T.W., Schmacke, N.A., Bridgeman, A., Rehwinkel, J., Zender, L., and Ablasser, A. (2017). Innate immune sensing of cytosolic chromatin fragments through cGAS promotes senescence. Nat Cell Biol 19, 1061–1070.

Gray, E.E., Treuting, P.M., Woodward, J.J., and Stetson, D.B. (2015). Cutting edge: cGAS is required for lethal autoimmune disease in the Trex1-deficient mouse model of Aicardi–Goutières syndrome. J Immunol 195, 1939–1943.

Gulen, M.F., Samson, N., Keller, A., Schwabenland, M., Liu, C., Glück, S., Thacker, V. V., Favre, L., Mangeat, B., Kroese, L.J., et al. (2023). cGAS–STING drives ageing-

related inflammation and neurodegeneration. Nature 620, 374–380.
Haag, S.M., Gulen, M.F., Reymond, L., Gibelin, A., Abrami, L., Decout, A., Heymann, M., van der Goot, F.G., Turcatti, G., Behrendt, R., et al. (2018). Targeting STING with covalent small-molecule inhibitors. Nature 559, 269–273.
Hong, Z., Mei, J., Li, C., Bai, G., Maimaiti, M., Hu, H., Yu, W., Sun, L., Zhang, L., Cheng, D., et al. (2021). STING inhibitors target the cyclic dinucleotide binding pocket. Proc Natl Acad Sci USA 118, e2105465118.
Hopfner, K.P., and Hornung, V. (2020). Molecular mechanisms and cellular functions of cGAS–STING signalling. Nat Rev Mol Cell Biol 21, 501–521.
Hu, S., Fang, Y., Chen, X., Cheng, T., Zhao, M., Du, M., Li, T., Li, M., Zeng, Z., Wei, Y., Gu, Z., Zhang, C., Sun, L., and Chen, Z.J. (2021). cGAS restricts colon cancer development by protecting intestinal barrier integrity. Proc Natl Acad Sci USA 118, e2105747118. doi: 10.1073/pnas.210574711.
Humphries, F., Shmuel-Galia, L., Jiang, Z., Zhou, J.Y., Barasa, L., Mondal, S., Wilson, R., Sultana, N., Shaffer, S.A., Ng, S.L., et al. (2023). Targeting STING oligomerization with small-molecule inhibitors. Proc Natl Acad Sci USA 120, e2305420120.
Ishikawa, H., Ma, Z., and Barber, G.N. (2009). STING regulates intracellular DNA-mediated, type I interferon-dependent innate immunity. Nature 461, 788–792.
Iwamura, T., Yoneyama, M., Yamaguchi, K., Suhara, W., Mori, W., Shiota, K., Okabe, Y., Namiki, H., and Fujita, T. (2001). Induction of IRF-3/-7 kinase and NF-κB in response to double-stranded RNA and virus infection: common and unique pathways. Genes Cells 6, 375–388.
Li, S., Hong, Z., Wang, Z., Li, F., Mei, J., Huang, L., Lou, X., Zhao, S., Song, L., Chen, W., et al. (2018). The cyclopeptide astin C specifically inhibits the innate immune CDN sensor STING. Cell Rep 25, 3405–3421.e7.
Liu, S., Cai, X., Wu, J., Cong, Q., Chen, X., Li, T., Du, F., Ren, J., Wu, Y.T., Grishin, N. V., et al. (2015). Phosphorylation of innate immune adaptor proteins MAVS, STING, and TRIF induces IRF3 activation. Science 347, aaa2630.
Liu, Y., Jesus, A.A., Marrero, B., Yang, D., Ramsey, S.E., Montealegre Sanchez, G.A., Tenbrock, K., Wittkowski, H., Jones, O.Y., Kuehn, H.S., et al. (2014). Activated STING in a vascular and pulmonary syndrome. N Engl J Med 371, 507–518.
Motwani, M., Pesiridis, S., and Fitzgerald, K.A. (2019). DNA sensing by the cGAS–STING pathway in health and disease. Nat Rev Genet 20, 657–674.
Nadeem, M.S., Kumar, V., Al-Abbasi, F.A., Kamal, M.A., and Anwar, F. (2020). Risk of colorectal cancer in inflammatory bowel diseases. Semin Canc Biol 64, 51–60.
Paludan, S.R., and Bowie, A.G. (2013). Immune sensing of DNA. Immunity 38, 870–880.
Rodero, M.P., Tesser, A., Bartok, E., Rice, G.I., Della Mina, E., Depp, M., Beitz, B., Bondet, V., Cagnard, N., Duffy, D., et al. (2017). Type I interferon-mediated autoinflammation due to DNase II deficiency. Nat Commun 8, 2176.
Seyedian, S.S., Nokhostin, F., and Dargahi Malamir, M. (2019). A review of the diagnosis, prevention, and treatment methods of inflammatory bowel disease. J Med Life 12, 113–122.
Shan, B., Hou, H., Zhang, K., Li, R., Shen, C., Chen, Z., Xu, P., Cui, R., Su, Z., Zhang, C., et al. (2023). Design, synthesis, and biological evaluation of bipyridazine derivatives as stimulator of interferon genes (STING) receptor agonists. J Med Chem 66, 3327–3347.
Shang, G., Zhang, C., Chen, Z.J., Bai, X., and Zhang, X. (2019). Cryo-EM structures of STING reveal its mechanism of activation by cyclic GMP–AMP. Nature 567, 389–393.
Shmuel-Galia, L., Humphries, F., Lei, X., Ceglia, S., Wilson, R., Jiang, Z., Ketelut-Carneiro, N., Foley, S.E., Pechhold, S., Houghton, J.M., et al. (2021). Dysbiosis exacerbates colitis by promoting ubiquitination and accumulation of the innate immune adaptor STING in myeloid cells. Immunity 54, 1137–1153.e8.
Song, J., Yang, R., Chang, J., Liu, Y., Lu, C., Chen, L., Guo, H., Zhang, Y., Fan, Z., Zhou, J., et al. (2023). Discovery and characterization of a novel cGAS covalent inhibitor for the treatment of inflammatory bowel disease. Acta Pharmacol Sin 44, 791–800.
Stetson, D.B., Ko, J.S., Heidmann, T., and Medzhitov, R. (2008). Trex1 prevents cell-intrinsic initiation of autoimmunity. Cell 134, 587–598.
Sun, X., and Kaufman, P.D. (2018). Ki-67: More than a proliferation marker. Chromosoma 127, 175–186.
Tanaka, Y., and Chen, Z.J. (2012). STING specifies IRF3 phosphorylation by TBK1 in the cytosolic DNA signaling pathway. Sci Signal 5, ra20.
Wang, J., Ba, G., Han, Y.Q., Ming, S.L., Wang, M.D., Fu, P.F., Zhao, Q.Q., Zhang, S., Wu, Y.N., Yang, G.Y., et al. (2020). Cyclic GMP-AMP synthase is essential for cytosolic double-stranded DNA and fowl adenovirus serotype 4 triggered innate immune responses in chickens. Int J Biol Macromol 146, 497–507.
Wang, Z., Guo, K., Gao, P., Pu, Q., Lin, P., Qin, S., Xie, N., Hur, J., Li, C., Huang, C., et al. (2021). Microbial and genetic-based framework identifies drug targets in inflammatory bowel disease. Theranostics 11, 7491–7506.
Wirtz, S., Popp, V., Kindermann, M., Gerlach, K., Weigmann, B., Fichtner-Feigl, S., and Neurath, M.F. (2017). Chemically induced mouse models of acute and chronic intestinal inflammation. Nat Protoc 12, 1295–1309.
Wottawa, F., Bordoni, D., Baran, N., Rosenstiel, P., and Aden, K. (2021). The role of cGAS/STING in intestinal immunity. Eur J Immunol 51, 785–797.
Wu, J., Sun, L., Chen, X., Du, F., Shi, H., Chen, C., and Chen, Z.J. (2013). Cyclic GMP-AMP is an endogenous second messenger in innate immune signaling by cytosolic DNA. Science 339, 826–830.
Yang, H., Wang, H., Ren, J., Chen, Q., and Chen, Z.J. (2017a). cGAS is essential for cellular senescence. Proc Natl Acad Sci USA 114, E4612–E4620.
Yang, R., Yuan, B.C., Ma, Y.S., Zhou, S., and Liu, Y. (2017b). The anti-inflammatory activity of licorice, a widely used Chinese herb. Pharm Biol 55, 5–18.
Yum, S., Li, M., Fang, Y., and Chen, Z.J. (2021). TBK1 recruitment to STING activates both IRF3 and NF-κB that mediate immune defense against tumors and viral infections. Proc Natl Acad Sci USA 118, e2100225118.
Zhang, C., Shang, G., Gui, X., Zhang, X., Bai, X., and Chen, Z.J. (2019). Structural basis of STING binding with and phosphorylation by TBK1. Nature 567, 394–398.
Zhao, B., Du, F., Xu, P., Shu, C., Sankaran, B., Bell, S.L., Liu, M., Lei, Y., Gao, X., Fu, X., et al. (2019). A conserved PLPLRT/SD motif of STING mediates the recruitment and activation of TBK1. Nature 569, 718–722.
Zhao, F., Zheng, T., Gong, W., Wu, J., Xie, H., Li, W., Zhang, R., Liu, P., Liu, J., Wu, X., et al. (2021). Extracellular vesicles package dsDNA to aggravate Crohn's disease by activating the STING pathway. Cell Death Dis 12, 815.
Zheng, J., Mo, J., Zhu, T., Zhuo, W., Yi, Y., Hu, S., Yin, J., Zhang, W., Zhou, H., and Liu, Z. (2020). Comprehensive elaboration of the cGAS-STING signaling axis in cancer development and immunotherapy. Mol Canc 19, 133.